Energy Reports 10 (2023) 1819–1832

Contents lists available at ScienceDirect

Energy Reports

journal homepage: www.elsevier.com/locate/egyr

Research paper

A novel optimized dynamic fractional-order MPPT controller using hunter pray optimizer for alleviating the tracking oscillation with changing environmental conditions

Eman Korany [a], Dalia Yousri [b], Hazem A. Attia [a], Ahmed F. Zobaa [c,*], Dalia Allam [b]

[a] Engineering Mathematics and Physics Dept., Faculty of Engineering, Fayoum University, Egypt
[b] Electrical Engineering Dept., Faculty of Engineering, Fayoum University, Fayoum, Egypt
[c] College of Engineering, Design & Physical Sciences, Brunel University London, Uxbridge, UB8 3PH, United Kingdom

ARTICLE INFO

Article history:
Received 18 June 2023
Received in revised form 11 August 2023
Accepted 20 August 2023
Available online xxxx

Keywords:
Photovoltaic reconfiguration
Partial shading
Hunger games search
Series–parallel PV
Total-cross-tied array

ABSTRACT

Introducing new control strategies in the photovoltaic (PV) system to continuously harvest the maximum power with the changes in environmental conditions is a crucial issue. Therefore, this paper proposes an efficient maximum power point tracker (MPPT) using the perspective of fractional calculus to provide an accurate dynamic response to the rapid changes in environmental conditions. The proposed control scheme is an integration between the fractional proportional–integral (FPI) controller and dynamic variable fractional-order perturb and observe (P&O) MPPT. To optimally identify the proposed MPPT controller parameters, a novel hunter-pray optimizer (HPO) is implemented as it is featured by its efficient balance between exploration and exploitation capacity. The proposed MPPT controller is examined with a series of experiments under dynamically changed environmental conditions. Furthermore, a detailed comparison is conducted versus a set of state-of-the-art including; incremental conductance (INC), basic P&O, MPPT-based particle swarm optimizer(PSO), MPPT-based Grey Wolf Optimizer(GWO), and MPPT-based cuckoo search algorithm (CSA). The results prove that the proposed MPPT is capable to track the global maximum generated power with a notable steady-state response and is almost free of oscillations which ensures an optimal adaptive dynamic performance in response to the rapid variation in the environmental conditions. Moreover, the proposed approach affirms its superiority compared to the set of state-of-the-art techniques in providing the highest maximum power levels in the shortest conversion time. The outcomes provide proof of the remarkable impacts of integrating fractional calculus in enhancing the dynamic response of the proposed MPPT because of the extra degree of freedom that enhance the flexibility of the MPPT.

1. Introduction

Lately, there has been an extraordinary expansion in employing photovoltaic (PV) as a renewable energy source owing to its merits as it is an environmental-friendly source, it is not costly in its maintenance, and it does not require any fuel as it uses the solar energy that is a gift and widely availability (Toumi et al., 2021). However, the PV systems' generated electrical power is based on the incident irradiation levels on its surface; thus, its harvested power is dynamically fluctuating with the change in environmental conditions (de Dieu Nguimfack-Ndongmo et al., 2022). To continuously work on the maximum harvested power from the PV system, implementing the maximum power point techniques (MPPT) has been considered a good solution for tracking the maximum power point (MPP) under changes in environmental conditions (Manna et al., 2023).

There are several research works for the MPPT techniques that have been established to identify the MPP of the PV system under changes in environmental conditions. The perturb and observe(P&O) MPPT is a widely implemented approach (Schoeman and Van Wyk, 1982). The tracking time and steady-state oscillations of P&O have relied on the perturbation step size. The small perturbation step size causes less oscillation with a slow response; meanwhile, the large perturbation step size may cause continuous oscillation around the MPP (Piegari and Rizzo, 2010). Hence, with the unexpected fluctuation in atmospheric conditions, the classical P&O algorithm has caused some deviation from MPP (Hohm and Ropp, 2003). In Femia et al. (2005), a solution for that deviating problem was proposed by suggesting a constraint on the perturbation step size ($\triangle D$) (Femia et al., 2007). In Jiang et al. (2012), a variable perturbation step size was used to improve the performance of P&O. However, the high value of $\triangle D$

* Corresponding author.
E-mail address: azobaa@ieee.org (A.F. Zobaa).

https://doi.org/10.1016/j.egyr.2023.08.038

Nomenclature

Acronyms

ANN	Artificial neural network
AO	Aquila optimizer
CSA	Cukoo search algorithm
DVPO	dynamic fractional variable order perturb and observe
FLC	fuzzy logic control
FOCV	fractional Open-Circuit Voltage
FPID	fractional order proportional–integral–derivative
FSCC	fractional Short-Circuit Current
GWO	Grey Wolf Optimizer
HPO	hunter pray optimizer
INC	incremental conductance
MPPT	maximum power point tracking
P&O	Perturb and Observe
PSO	Particle Swarm Optimization
PVPS	Photovoltaic Power System
SDM	single diode model
SMA	slime mold algorithm
MPP	maximum power point

Variables

ΔV	change in PV voltage
Δ I	change in PV current
λ	fractional order integral
A	diode ideality factor
D	duty cycle
$e(t)$	error signal
I	PV current
Io	diode saturation current
Iph	photo-generated current
K	the Boltzmann constant($1.3806503 \times 10^{-23}$ J/K)
K_i	integration constant factor
K_p	proportional constant factor
m	scaling factor of DVPO
Np	parallel strings
Ns	cells in a series string
NU	search agents number
P	output power from PV panel
q	electron charge($1.60217646 \times 10^{-19}$ C)
Rs	series resistance
Rsh	shunt resistance
T	the temperature of the solar cell in kelvin(K)
V	output voltage from PV panel
V_{out}	output voltage from boost converter
V_{pv}	PV voltage
V_{ref}	output voltage from MPPT
x_i	position of the animal(hunter or pray)

is essential to minimize the deviation from MPP during any remarkable shift of insolation to avoid the increase in power loss at a steady state. Another solution has been described in Sera et al. (2008), where upper and lower thresholds have been allowed for the power to be changed (P), but this solution was not an ideal solution due to the constraints on the threshold values of P, which are mostly dependent on the amount of change in insolation. The classical incremental conductance(IC) technique was proposed to tackle the classical P&O oscillation issue in Wasynezuk (1983). Then updated variants of IC were proposed in Phang et al. (1984), Won et al. (1994), Hussein et al. (1995). To simplify the MPPT, the fractional Short-Circuit Current (FSCC) technique was carried out by Salameh et al. (1991), and the fractional Open-Circuit Voltage (FOCV) technique was implemented in Pandey et al. (2007). However, the implementation of FSCC leads to the ineffective tracing of MPP due to oscillatory performance at various irradiation levels (Fapi et al., 2021). For the FOCV performance, it relies on data collecting before showing a constant voltage reference, and this can vary depending on the operating condition (Baimel et al., 2019). The oscillations associated with implementing these conventional MPPT techniques have proved that these classical approaches cannot have the ability to dynamically responded with sudden variations in solar irradiation. Therefore, there was a persistent need to propose efficient and reliable approaches to provide a fast and smooth response (Abdallah et al., 2023).

Seeking to detect the MPP properly and enhance the MPP tracking process, an artificial neural network (ANN) was used (Jyothy and Sindhu, 2018). However, there were some drawbacks in utilizing ANN due to the long training time in tackling the vast amount of data, leading to a complicated network and a lower MPPT accuracy (Abdallah et al., 2023). The fuzzy logic control (FLC) was adopted in Narendiran et al. (2016) for the more profitable harvesting of MPP of the PV system. Yet, FLC could not respond to the rapid dynamic changes of irradiation (Boukezata et al., 2016). Therefore, it was very crucial to introduce MPPT in conjunction with other strategies to obtain more appealing results and robust MPPT control (Fathi and Parian, 2021). That is why bio-inspired and population-based optimization algorithms were proposed to be merged into MPPT control strategies. Several types of these optimization techniques were proposed including memetic salp swarm algorithm (Yang et al., 2019b), dynamic leader based tracker (Yang et al., 2019a), swarm-based optimization (Wasim et al., 2022), improved firefly algorithm (Farayola et al., 2022), and mayfly optimization algorithm (Mo et al., 2022) and other approaches were employed in Mao et al. (2020), Yang et al. (2020). These approaches have affirmed their effectiveness with various atmospheric conditions; nevertheless, they have a poor dynamic response, extensive processes, and computational complexity problems. Furthermore, compromising between convergence accuracy and convergence speed, as well as adjusting the parameters of these algorithms.

Furthermore, recent works for MPPT were proposed to combine two advantages of different MPPT techniques for mitigating the drawbacks of the previous control techniques, such as a combination of a meta-heuristic technique as artificial bee colony with classical P&O, as reported in Pilakkat and Kanthalakshmi (2020). Another approach of integrating the proportional–integral (PI) controller and a genetic algorithm (GA) was proposed in Zaghba et al. (2019). Other combinations for MPPT were proposed such as P&O-PI and fuzzy controllers optimized by PSO and GA (Borni et al., 2017), MPPT-based IC integrated with a PI controller (Hsieh et al., 2012), integration proportional–integral–derivative (PID) with P&O (Sahoo et al., 2020), and PID-based MPPT controller optimized by ant-lion optimizer(ALO) (Sahu and Shaw, 2018).

Based on the literature, the PID controller variants were integrated with the MPPT as an alternative controller (Prasad et al., 2022). These controllers were utilized with different converters such as buck (Pandey et al., 2008), boost (Bui et al., 2022). The latest variant of these controllers is the fractional-order-based controllers, which prove their efficiency and reliability

in many control systems (Baleanu et al., 2011; Soliman et al., 2019). This new avenue offers better modeling of the control system (ElSafty et al., 2020). The fractional-order proportional–integral–derivative (FOPID) controller proved its superiority as one of the best newly developed fractional calculus-based controllers in many applications (Aboelela et al., 2012). The FOPID has two additional parameters compared to the integral-based PID that are known by the fractional order derivative (μ) and the fractional order integral (λ). These additional parameters could enhance the flexibility of the control system. In Bouakkaz et al. (2020), a technique of fractional order controller tuned by swarm optimization was used integrated with classical P&O under various environmental operating conditions. However, utilizing the fractional controller with classical P&O still cannot achieve zero oscillation in tracking the MPP while the sudden changes in the environmental conditions occur.

To fulfill the research gaps and tackle the drawbacks in the previous MPPT, this paper proposes a novel integrated MPPT controller-based fractional calculus to enhance the MPP tracking, minimize the oscillation and improve the dynamic response to sudden changes in environmental conditions. The proposed approach is an integration between the fractional variable-order P&O (DVPO) and FPI. The parameters of the proposed control are adaptively tuned using one of an efficient swarm-based-optimizer named hunter–prey optimizer(HPO). The HPO is selected as it featured by its efficient balance between exploration and exploitation capacity, it does not require external tunable parameters, and it has produced very competitive results compared to the other well-known and innovative optimization techniques in several applications (Ramadan et al., 2022; Naruei et al., 2022; Wang et al., 2023). The optimized DVPO integrated with FPI is validated using several series of experiments. Moreover, it is compared with a set of integer and fractional-order variants of PID coupled with the classical P&O. For providing a comprehensive analysis; the proposed approach is compared with the state-of-the-art techniques including, MPPT-based aquila optimizer (AO), MPPT-based slime mold algorithm (SMA), INC, MPPT-based particle swarm optimizer(PSO), MPPT-based Grey Wolf Optimizer(GWO), and MPPT-based cuckoo search algorithm (CSA). The harvested maximum power, time of convergence, and oscillations are highlighted as evaluation matrices. The outcomes provide proof of the remarkable impacts of integrating fractional calculus in enhancing the dynamic response of the proposed MPPT because of the extra degree of freedom that enhances the flexibility of the MPPT. The main contribution of this work is listed as follows:

- Proposing a novel reliable MPPT based on the perspective of the fractional calculus for providing an extra degree of freedom during the MPP tracking process, accordingly an integrated fractional variable-order P&O (DVPO) and fractional-order proportional–integral (FPI) controller is developed.
- Employing the hunter–prey optimizer(HPO) to identify the proposed control parameters optimally.

2. System element description

The main elements of the MPPT-based PV system are PV panels, DC–DC boost converter, control system, and load as shown in Fig. 1. The PV system is composed of an MPPT-based DVPO and integrated with the fractional PI approach. When the source impedance equals the load impedance, maximum power is moved from the source to the load, according to the maximum power transfer theory. A boost DC–DC voltage converter is used to modify the PV panel voltage so that it can function around the MPP. The duty cycle of the converter can be adjusted to provide load matching. Under the dynamic changes in the environmental conditions, the converter duty cycle must be modified to extract maximum power from the PV system and enhance efficiency (Reisi et al., 2013; Rezk and Eltamaly, 2015).

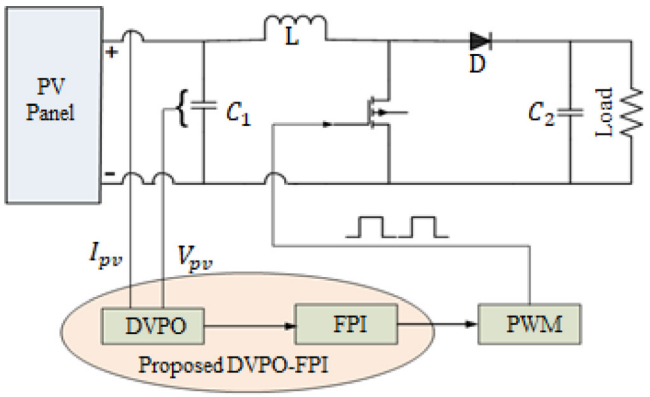

Fig. 1. Block diagram for proposed DVPO-FPI MPPT.

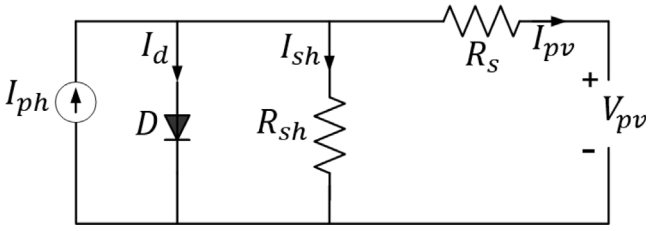

Fig. 2. Equivalent circuit of SD-PV model.

2.1. Mathematical representation of PV panel

In a PV solar panel, solar sunlight is converted into electrical power via the photoelectric effect. Fig. 2 depicts a single-diode model (SDM) for representing the PV module behavior, the equivalent circuit composed of a nonlinear current source to represent the generated current of the solar cell in parallel with a diode D and shunt resistance R_{sh}. The parallel branches are connected in series with resistance R_s as illustrated in Fig. 2. Regarding the SDM parameters, they are collected from the literature for PV parameters estimation (Hansen, 2015; Kang et al., 2018).

As illustrated in Fig. 2, the leakage current is caused by the shunt resistance. The ohmic losses and material resistivity at contacts are represented by the series resistance(R_s). The relationship between the output voltage (V_{pv}) and the generated current (I_{pv}) is given by Eq. (1)(Hamid et al., 2016).

$$I_{pv} = \left[I_{ph} N_p - I_o N_p \left[e^{\frac{q\left(\frac{V_{pv}}{N_s} + \frac{I_{pv} R_s}{N_p}\right)}{AkT}} - 1 \right] - \frac{\frac{V_{pv} N_p}{N_s} + I_{pv} R_s}{R_{sh}} \right] \quad (1)$$

Where I_o, I_{ph}, A, I_{pv}, V_{pv}, N_p and N_s represent diode saturation current, photo-generated current, diode ideality factor, the output current, output voltage from PV unit, parallel strings and series cells in the string, respectively.

The I-V and P-V characteristics of the PV unit under various environmental condition of 1000, 750, 500, and 250 W/m^2 and 25 °C can be illustrated in Fig. 3.

2.2. DC–DC converter

The converter used in this work is a boost (step-up) DC–DC Converter, as shown in Fig. 4. The boost converters are frequently

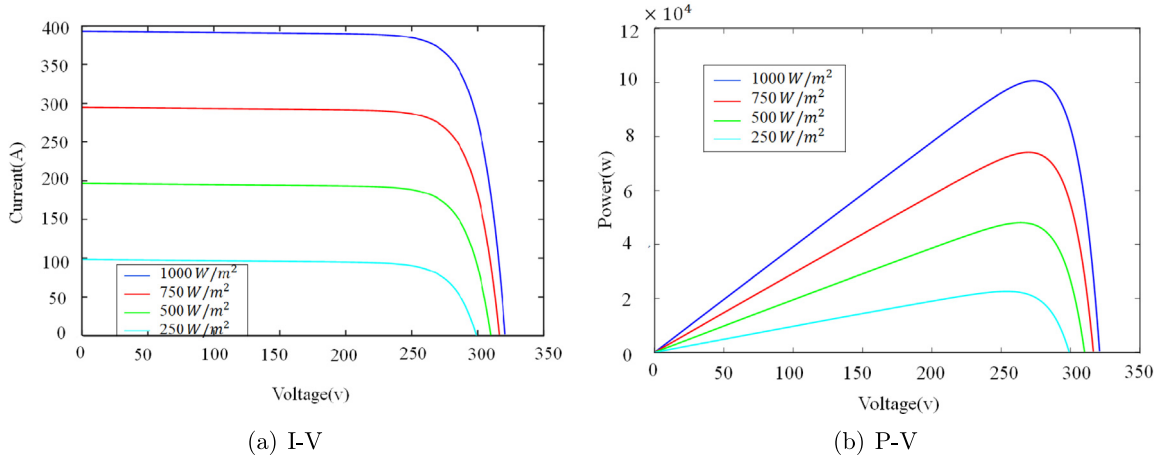

(a) I-V (b) P-V

Fig. 3. The I-V curve and P-V curve of PV module at different radiation levels.

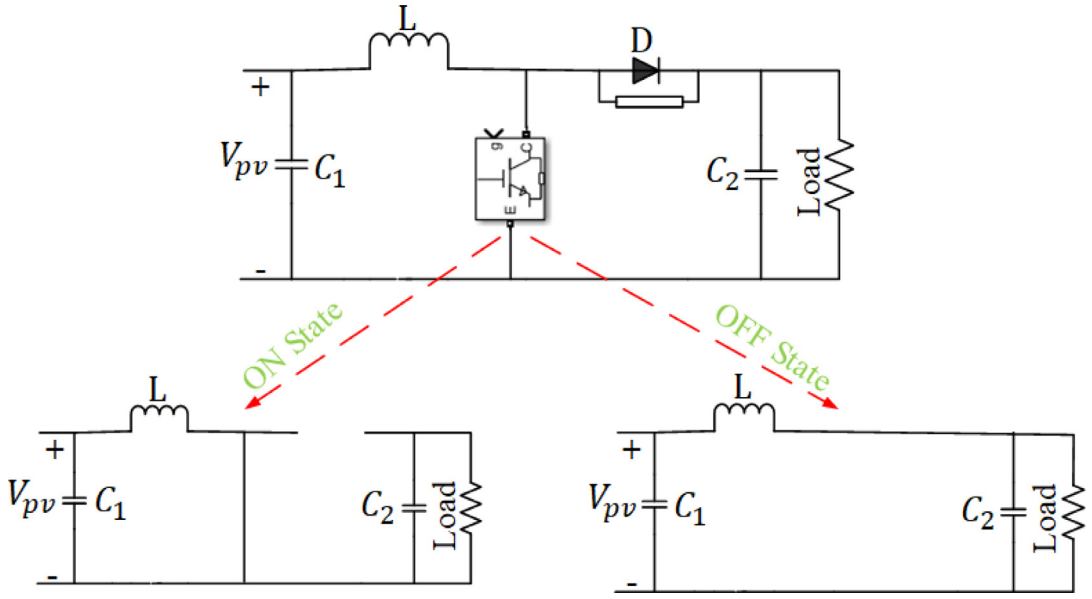

Fig. 4. The boost DC–DC converter and its operation.

used to increase the voltage of solar panels by altering the duty cycle of the MOSFET switch. An input capacitor is added to the PV panel's input side to reduce the high-frequency harmonic components (Rezk and Eltamaly, 2015). The duty cycle (D) is characterized as the period of time during which the switch is ON, with values between 0 and 1. To extract the maximum power from the PV system, the duty cycle of the boost converter is continuously monitored. In case of changes in radiations, the boost stage is operated at varying duty cycles depending on the control signal coming from the MPPT. The converter voltage is calculated as given below:

$$V_{out} = \frac{V_{pv}}{1 - D} \tag{2}$$

where V_{out} is the output voltage at the terminal of DC–DC boost converter and V_{pv} is the output voltage at the PV panel terminal. The D is the Duty cycle that its value can be calculated from the following relation

$$D = \frac{T_{ON}}{T_{ON} + T_{OFF}} \tag{3}$$

Where T_{ON} is the on-state period and T_{OFF} is the off-state period.

3. Basic Perturb and Observe algorithm (P&O)

The maximum power output of the PV module is affected by environmental changes, either changes in cell temperature or solar irradiation. In PV systems, the MPPT technique is used to extract the MPP under variable conditions. The P&O technique boosts or reduces the module voltage to find the maximum output power as in Fig. 5. If the differentiation of PV power divided by the differentiation of PV voltage (dP/dV) is positive, which is to the left of the MPP, the voltage is increased to obtain the MPP. When dP/dV is negative, the voltage is lowered to approach the MPP as illustrated in Table 1. In classical P&O MPPT, the movement step is fixed. The P&O approach is the most basic and uncomplicated to use. The approach, however, is not optimal for quick changes in environmental conditions. Because of the slow tracking with the fixed step size, The output voltage and current signals oscillate in the steady state (A. Elbaset et al., 2015). By utilizing a dynamic variable step size, the oscillatory behavior can be decreased.

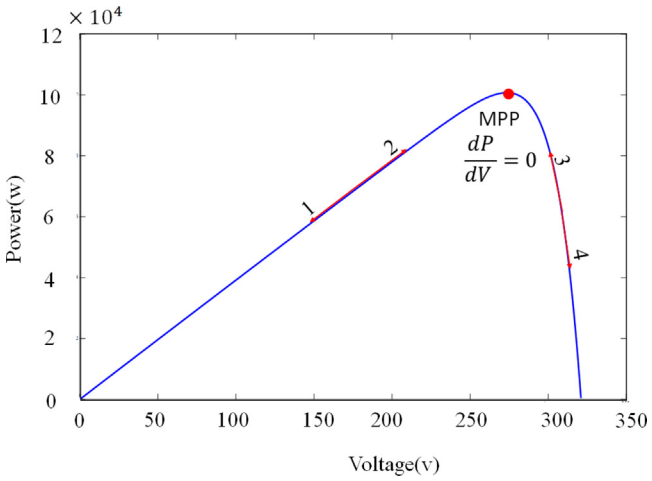

Fig. 5. The P&O algorithm positioning.

4. The proposed MPPT-based DVPO and FPI

In the classical P&O MPPT technique, the perturbation step of the duty cycle has a constant effort. If this step is large, the dynamic response will be quick, but the problem of steady-state oscillations will appear. The oscillation will improve if a small step is used, but the dynamic response will become slower. Therefore, balancing these two aspects (dynamic response and the oscillations) became a significant flaw for the classical P&O MPPT technique. To overcome this drawback, the constant step size is replaced by the slope of power to voltage(dP/dV) and two different dynamic step size increments, as shown in Eqs. (4) and (5)

$$\text{First step} = \frac{ma}{I}\left|\frac{dP}{dV}\right| \tag{4}$$

Table 1
P&O positioning and action.

Position	dP/dV	Action
1	−	Increase Voltage
2	+	Increase Voltage
3	+	Decrease Voltage
4	−	Decrease Voltage

$$\text{Second step} = \frac{mb}{I}\left|\frac{dP}{dV}\right| \tag{5}$$

where 1 is withdrawn from the interval of [a b].

Selection of the proper steps for tracking MPP relies on the current variation (ΔI). The increase in solar irradiation leads to increasing in current(I). As a result, the step size gradually grows larger. Because the normalization coefficient (a) is less than 1, Eq. (4) is utilized. However, as the solar irradiation level lowers, the current also decreases, resulting in a reduction in the step size. Because the normalization coefficient (b) is bigger than 1, Eq. (5) is utilized. The scaling factor(m), which is a constant in scalar form, acts as a crucial parameter for the DVPO MPPT technique. Its value affects the process of MPP tracking and it takes value from 0 to 0.1. The flowchart of the dynamic fractional-variable order perturb and observation (DVPO) is shown in Fig. 6.

As illustrated in Fig. 1, the fractional-order proportional-integral (FPI) controller is integrated with the MPPT-based DVPO to send the settings for the DC–DC converter. Fig. 7 shows the FPI controller's block diagram. This controller is defined by (PI^{λ}). The FPI controller is a more advanced version of the integral-order PI controller. The fractional order controller tuning parameters improve the controller's robustness compared to the integer controller. As a result, the new parameter provides greater flexibility and improves the closed-loop system's dynamic behavior. The FPI controller differential equation is given below,

$$u(t) = (K_p + K_i D_t^{-\lambda})e(t) \tag{6}$$

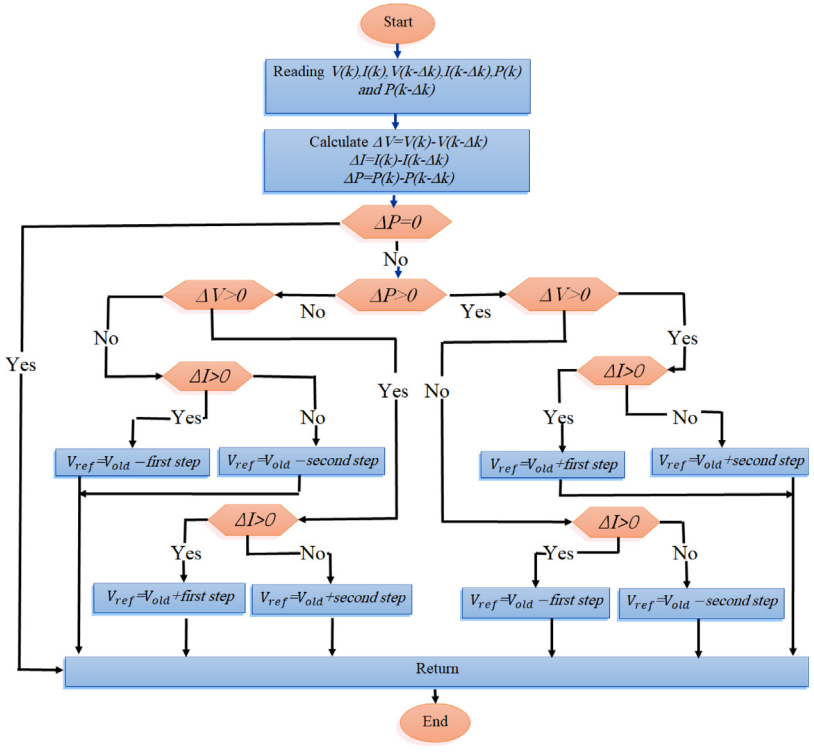

Fig. 6. The flow chart of the dynamic fractional variable order P&O MPPT algorithm.

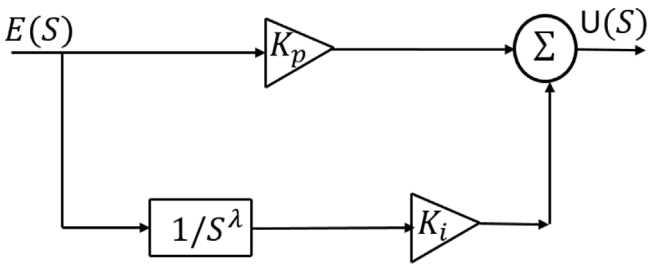

Fig. 7. The block diagram of FPI controller.

where $e(t)$ is the error signal, $u(t)$ is the control signal, K_p is the proportional constant factor and K_i is the integration constant factor. The fractional order integral λ is an arbitrary real number. It is worth mentioning that the integral-order PI controller is a particular case of the fractional controller when $\lambda = 1$. Using Eq. (6), the transfer function of the FPI controller is given by:

$$\frac{U(S)}{E(S)} = K_p + K_i S^{-\lambda} \tag{7}$$

5. Adaptive tuning the parameters of proposed MPPT-based DVPO with FPI

To optimally readjust the parameters of the proposed MPPT ($K_p, K_i and \lambda$) with the changes in the environmental conditions, hunter–prey optimization is adopted using the error function between the measured voltage and the output voltage of PV as exhibited in Fig. 10. The mathematical formulation of the objective function is given below:

$$e(t) = V_{pv} - V_{ref} \tag{8}$$

The mechanism of the proposed MPPT algorithm is extracting the V_{ref} by increasing or decreasing the PV voltage with dynamic steps that depend on ΔV and ΔI until it reaches the maximum power point as illustrated in the flowchart in Fig. 6. A detailed description of the implemented HPO is presented below:

5.1. Hunter–prey optimization algorithm

In the hunter–prey optimization algorithm (Naruei et al., 2022), the hunter is searching for food by chesting the prey; meanwhile, the prey escapes to safe places to save its life. Accordingly, in this algorithm, the agents continuously search for an updated optimal solution as depicted in Fig. 8. Naruei et al. (2022) modeled a set of mathematical formulations for tailoring the HPO as described below:

- Initialization: The initial population is defined as $(\overrightarrow{x}) = (\overrightarrow{x_1}, \overrightarrow{x_2}, \ldots \overrightarrow{x_n})$ at random, and the objective function for all members of the population is calculated as $(\overrightarrow{O}) = \{O1, O2, \ldots .On\}$ A set of rules and approaches prompted by the suggested algorithm are used to manage and guide the population in the search space. This process continues until the algorithm is terminated. Each iteration updates the location of each population member according to the algorithm's criteria, and the position is changed by the objective function. As a result of this approach. The position of each animal of the initial population is randomly constructed in the search space by Eq. (9).

$$x_i = rand(1, dim). * (up - low) + low \tag{9}$$

where x_i represents the position of the animal(hunter or pray), low represents the problem variables' lower boundary, up represents the problem variables' upper boundary, and dim represents the problem's number of variables. The lower and higher limits of the search space are defined by Eq. (10).

$$low = [low_1, low_2, \ldots .., low_d], up = [up_1, up_2, \ldots .., up_d] \tag{10}$$

After calculating the first population and defining each member's position, the fitness of each solution is calculated using the objective function $O_i = f(\overrightarrow{x})$.

- Updating the hunter's position or prey: The fitness function indicates if a solution is excellent or terrible, but the best solution is not achieved in one run. In order to direct the search members to the best spot, a search method must be created and used repeatedly. Exploration and exploitation are typically the two steps in the search process. Exploration is the algorithm's proclivity for highly unpredictable behavior, resulting in dramatically different solutions. Significant modifications in solutions necessitate the further study of the area of search and the identification of interesting locations. Following the discovery of interesting locations, random actions must be decreased so that the approach can search around them, which is referred to as exploitation. Eq. (11) is suggested for the prey search mechanism.

$$x_{i,j}(t+1) = x_{i,j}(t) + 0.5[(2CZP_{pos(j)} - x_{ij}(t)) + (2(1-C)Z_{\mu(j)} - x_{ij}(t))] \tag{11}$$

where $x(t)$ represents the current hunter location, $x(t+1)$ represents the next hunter location, P_{pos} represents the prey location, μ represents the average of all locations, and Z represents an adaptable element determined by Eq. (12).

$$B = \overrightarrow{R_1} < C; INDX = (B == 0); Z = R_2 \otimes INDX + \overrightarrow{R_3} \otimes (\sim INDX). \tag{12}$$

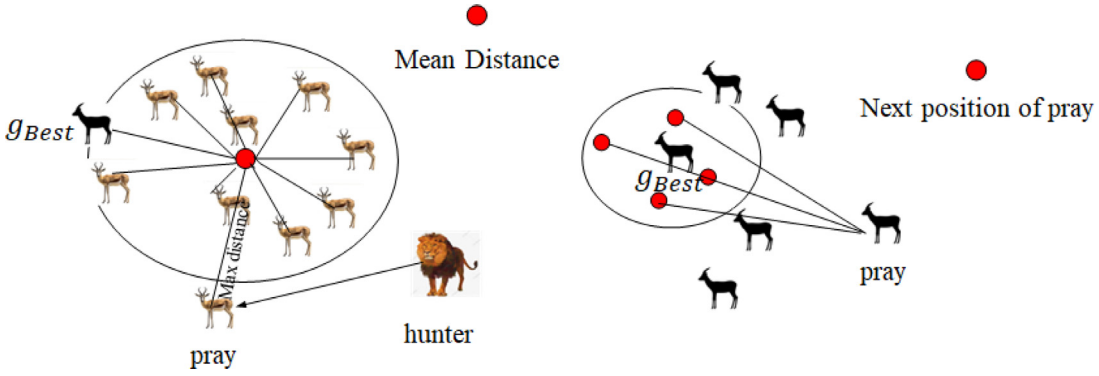

Fig. 8. The left picture is hunter behavior, The right picture is prey behavior, and the next position of prey.

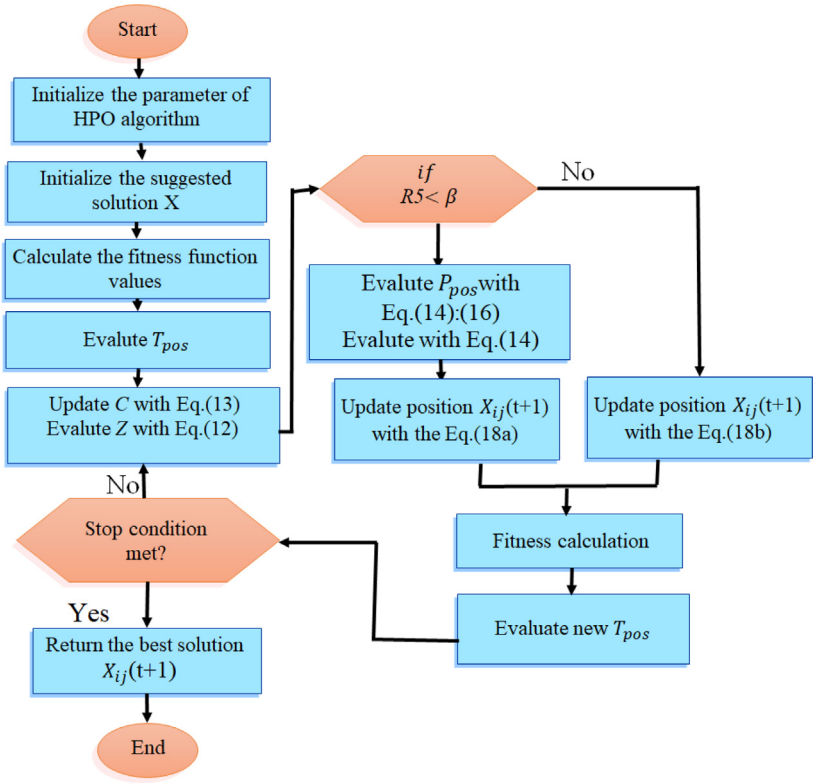

Fig. 9. The flowchart of the proposed HPO algorithm.

where $\overrightarrow{R_1}$ and $\overrightarrow{R_3}$ are vectors take values from 0 to 1, B is a vector takes values equal to the number of controller variables, R_2 is an integer from 0 to 1, and $INDX$ is the index numbers of the vector $\overrightarrow{R_1}$ that accepts the criteria ($B == 0$). C is the exploration–exploitation balance element with a value that falls from 1 to 0.02 during running the approach. The value of C is computed as follows:

$$C = 1 - it(\frac{0.98}{MAXIt}). \tag{13}$$

where It is the momentary iteration value, and MAX is the most iterations possible. The location of the prey P_{pos} is calculated as indicated in Fig. 8 by first calculating the mean of all locations (μ) using Eq. (14), after that calculating each search agent's distance from this mean location.

$$\mu = \frac{1}{n}\sum_{i=1}^{n}\overrightarrow{x_i}. \tag{14}$$

the distance is calculated by Euclidean distance from Eq. (15)

$$D_{euc(i)} = (\sum_{j=1}^{d}(x_{ij} - \mu_j)^2)^{0.5}. \tag{15}$$

the most distant search agent from the mean of placements is deemed prey P_{pos}, according to Eq. (16).

$$\overrightarrow{P_{pos}} = \overrightarrow{x_i} \,|iissorted D_{euc}(Lbest). \tag{16}$$

where $Lbest = round(C * NU)$ and NU is the search agents number. Prey tries to run when it is attacked and find a safe area, as seen in Fig. 8 The optimum safe location is assumed to be the optimal global location since the prey will have a better chance of surviving as a result, and the hunter will be free to choose another prey. To update the prey position, Eq. (14)is proposed.

$$x_{i,j}(t+1) = T_{pos(j)} + CZcos(2\pi R_4) * (T_{pos(j)} - x_{i,j}(t)) \tag{17}$$

Where T_{pos} is the optimum global, and R_4 is an arbitrary number in the range $[-1, 1]$. in this algorithm, to choose the hunter and prey, we join Eqs. (14) and (17) as Eq. (18)

$$x_{i,j}(t+1) = x_{i,j}(t) + 0.5[(2CZP_{pos(j)} - x_{ij}(t)) + (2(1-C)Z_{\mu(j)} - x_{ij}(t))] \quad if\ R_5 < \beta \tag{18a}$$

$$OR \quad x_{i,j}(t+1) = T_{pos(j)} + CZcos(2\pi R_4) * (T_{pos(j)} - x_{i,j}(t)) \quad else \tag{18b}$$

where R_5 is an arbitrary number between 0 and 1, and β is a regulating factor with a value of 0.1 in this work. The flow chart of the proposed algorithm is shown in Fig. 9.

6. Discussion and simulation results

The response of the proposed MPPT control scheme is examined in this section using a set of case studies for different levels of incident irradiation on the PV system. The implemented system is depicted in Fig. 10 using Matlab/Simulink platform. The modeled equivalent circuit of the PV module is based on the SDM of Fig. 2. The utilized five parameters of the SDM at nominal conditions are as follows: $I_{ph} = 5.9606A$, $I_o = 5.2622e^{-9}$ A, $A = 1.25$, $R_{sh} = 819.13001\ \Omega$, $R_s = 0.083029\ \Omega$, $N_s = 5$ and $N_p = 66$. The parameters of the boost converter are $L = 0.005H$, $C_1 = 100e^{-6}$, and $C_2 = 12000e^{-6}$. The number of iterations and population size of HPO are 10 and 5, respectively. The analyses and discussions have been conducted in sequential stages of investigation to clarify the importance of proposing an optimized fractional-order controller along with the dynamic fractional variable order P&O MPPT. The simulations and analyses are executed

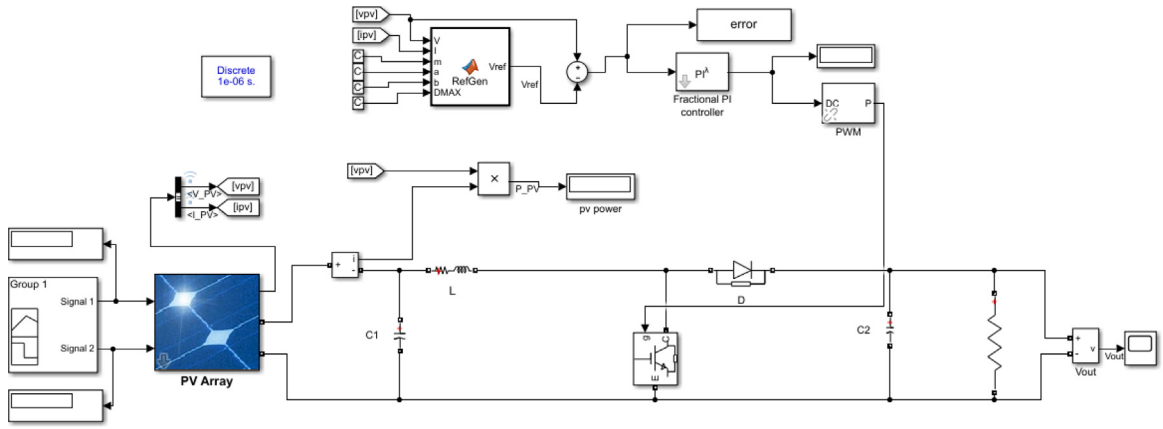

Fig. 10. The MATLAB/Simulink model of the proposed system.

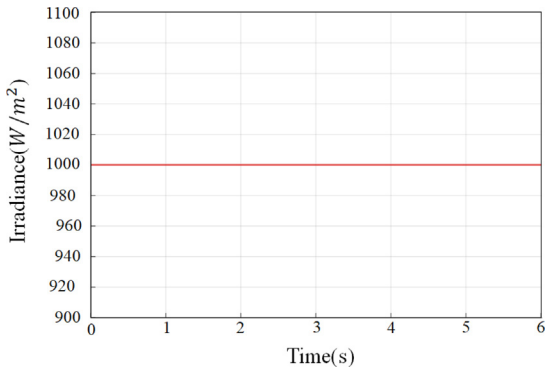

Fig. 11. Radiation pattern of (1000 W/m^2).

on MATLAB/Simulink 2020a using a personal computer with an Intel(R)CoreTMi5 CPU at 3.20 GHz and 8 GB of RAM. The solver is ode 45 (Dormand-Prince) with a variable-step size.

- First stage of the investigation (using integral controllers with classical P&O):
  The PV unit is subjected to radiation of 1000 W/m^2(see Fig. 11): this stage has been established by using several types of integral controllers, including PI, PD, and PID, coupled with the classical P&O technique, to investigate their performance while tracking MPP. The implemented controller performances in Fig. 12(a) illustrate that the PI controller has a remarkable response compared to the other controllers. However, the oscillations are still considerably large, as shown in the figure.
- Second stage of the investigation (using fractional controllers with classical P&O). The PV unit surface receives radiation of 1000 W/m^2:
  this stage demonstrates the results of the fractional variants of PI (FPI), PD (FPD), and PID (FPID) along with the classical P&O. The responses of the implemented controllers are plotted in Fig. 12(b). By examining the plotted curves in Fig. 12(b), it is evident that the FPI has the best performance compared to the FPD and FPID. Comparing the responses of PI and FPI in Fig. 13 reveals that the FPI and PI are highly comparable controllers in tracing the MPP. It is worth mentioning that notable oscillation is still detected in their responses.

- Third stage (using the dynamic fractional variable order P&O instead of the classical P&O):
  Based on the previous observations in the first and second stages, it is obvious that the PI controller and FPI controller are the most compatible approaches in extracting the best output voltages from the converter to the load. However, the controllers' responses still suffer from detectable oscillations until detecting the corresponding voltage to the MPP. Accordingly, enhancing the classical P&O is the current stage for handling the oscillation problem. For adaptive tuning of the proposed controller parameter, the HPO algorithm is executed. In this stage, the comparison between the DVPO-FPI controller and the DVPO-PI controller is performed using two patterns of radiation to validate the proposed strategy.
- The first pattern of radiation is (1000–800–600 W/m^2): In this pattern, the solar radiation has been changed in three levels, 1000 W/m^2 for the first 3 s; then it is reduced to 800 W/m^2 until the time of 5 s, and the last radiation level is 600 W/m^2 from time of 5 s to 6 s as depicted in Fig. 14. Fig. 15 displays the output voltage responses of MPPT controllers based on the optimized DVPO with FPI and PI controllers. The implemented MPPT responses illustrate that the dynamic fractional variable order (DVPO) has the ability to provide real-time reference voltage, which could improve the oscillatory response of the controller and increase its speed in tracking the changes in the environmental conditions. The proposed MPPT-based DVPO-FPI consumes about 0.083 s to reach the steady state; meanwhile, the MPPT-based DVPO-PI reaches at 0.104 s as illustrated in Fig. 15. Moreover, the proposed approach has the ability to determine the output voltage corresponding to the MPP accurately compared with the DVPO-PI, in turn maximizing the output energy. The DVPO-FPI converges to 493.55 V at 1000W/m^2, which is highly matched to the theoretical MPP value; meanwhile, the DVPO-PI converges to a lower value of 483.87V at 1000W/m^2. In radiation level 800 W/m^2, the DVPO-FPI reaches a steady state voltage equal to 445.16V that is close to the theoretical MPP value, whereas the DVPO-PI steady state voltage is 432.26V. Similarly, the DVPO-FPI shows the best response for the last radiation level of 600 W/m^2, FPI reaches a steady state voltage equal to 377V; however, the DVPO-PI steady state voltage is 358.92V. Based on the previous observations, one can conclude that the implementation of an optimized fractional controller variant rather than the integer one with the DVPO leads to better accuracy and faster response.

- The second pattern of radiation is (700–500–900 W/m^2): For more validation of the proposed strategy, the DVPO-FPI and DVPO-PI controllers have been tested at different

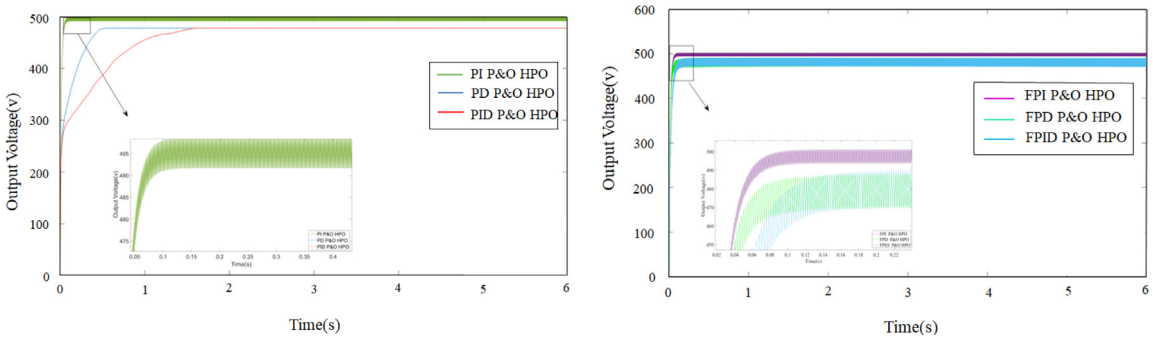

Fig. 12. The output voltages responses of the MPP controllers in cases of (a) integer-order controller (b) fractional-order controllers.

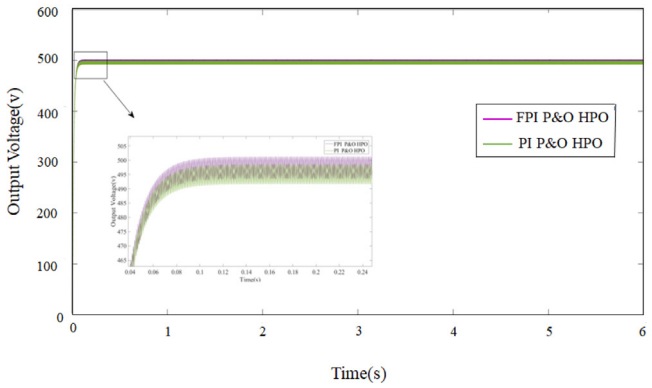

Fig. 13. The output voltages responses of optimized MPPT controller using HPO while coupled with FPI-P&O controller and PI-P&O controller.

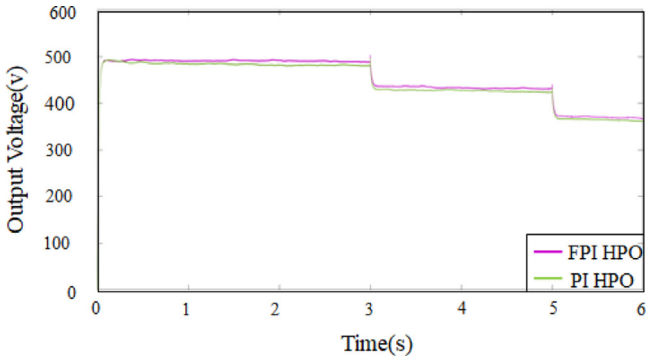

Fig. 15. The output voltage responses of optimized MPPT controller using HPO while coupled with DVPO-FPI controller and DVPO-PI controller in case of pattern 1.

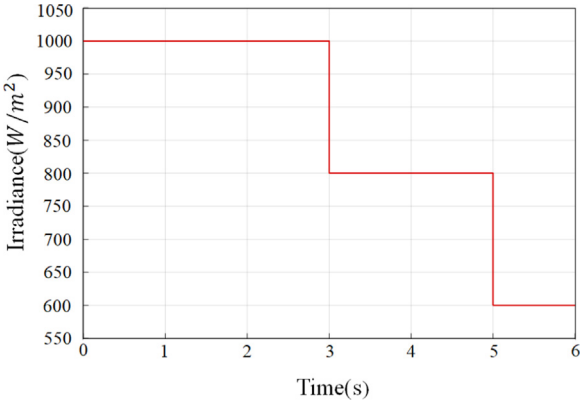

Fig. 14. Pattern 1: radiation levels of (1000–800–600 W/m^2).

levels of radiation of 700–500–900 W/m^2 as illustrated in Fig. 16. The considered pattern is investigated to prove the efficiency of DVPO-FPI versus DVPO-PI in the speed of control action in response to the changes in radiation levels and the quality of the controller in mitigating the oscillations, in addition to the accuracy of detecting the output voltage corresponding to MPP. The controllers' responses are drawn in Fig. 17. The plotted curves reveal the efficiency of the DVPO-FPI in detecting the corresponding voltage to the MPP with fast responses as it settled to the voltage of 402.5 V at 0.0625 s for the first level. Meanwhile, the DVPO-PI converges to 380 V at 0.0729 s For the other levels (500–900 W/m^2) throughout the pattern, the DVPO-FPI offers a fast and accurate response.

Based on the previous discussions, the MPPT using the DVPO-FPI proves its efficiency and reliability in detecting the voltage corresponding to MPP. To provide a shred of evidence for using the HPO, the HPO performance has been evaluated versus set-of-state-of-the art techniques, including; the slime mold algorithm (SMA) and Aquila optimizer (AO). Three irradiation levels are considered in this evaluation stage; that are 1000 W/m^2, (850–700) W/m^2, and (900–600) W/m^2 as shown in Fig. 18. The results of DVPO-FPI based on the three algorithms (HPO, SMA, and AO) are drawn in Fig. 19. The results of the figure divulge that the HPO algorithm outperforms the other tested algorithms in accuracy and the speed of conversion as well as the execution times, which proves the efficiency and the robustness of the recommended algorithm to be implemented within the proposed strategy.

The previous discussions prove that utilizing a fractional-order controller instead of the integral one in the control process of MPPT of PV system enhances the performance of the controller remarkably owing to the extra degrees of freedom. The extra degrees of freedom endorse the controller's response to converging to the MPP efficiently. Moreover, applying the HPO optimization technique for the identification of the fractional controller parameters shows an outstanding effect in its accuracy. Furthermore, combining the optimized fractional control with the dynamic fractional variable order P&O provides the reference voltage in response to any dynamic changes in the operating conditions,however identifying the parameters of the proposed fractional based MPPT is considered the main challenge.

Table 2
The proposed response versus the literature for the first case.

Radiation level	Comparison	Proposed	PSO	GWO	INC	P&O	CSA
550 W/m^2	P_{max} (W)	51910	51010	46630	50110	50310	50580
	Time for convergence (s)	0.074	0.195	0.117	0.0826	0.554	0.681
	Oscillation	No	High	Medium	Low	Low	High
300 W/m^2	P_{max} (W)	26690	26450	26470	26070	26020	16900
	Time for convergence (s)	0.063	0.096	0.085	0.079	0.1	0.147
	Oscillation	No	Low	No	No	No	No
750 W/m^2	P_{max} (W)	69070	59050	52490	69370	69067	61290
	Time for convergence (s)	0.069	0.324	0.127	0.073	0.076	0.304
	Oscillation	No	High	Medium	Low	Low	High

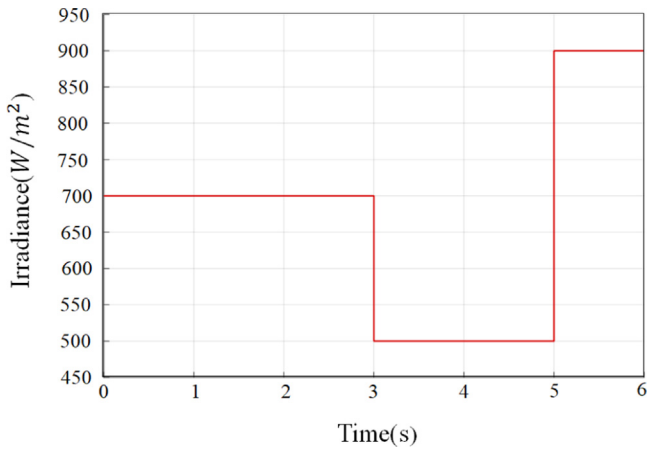

Fig. 16. Pattern 2: radiation levels of (700–500–900 W/m^2).

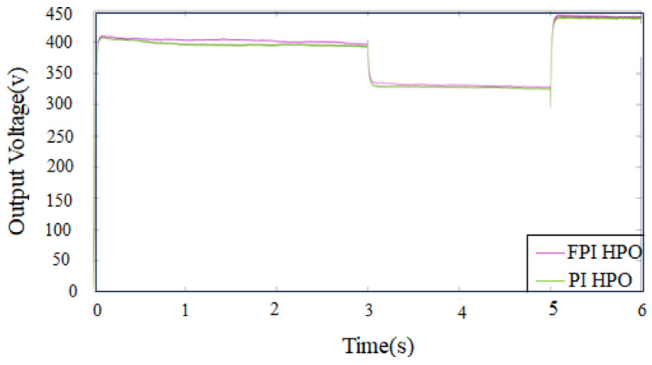

Fig. 17. The output voltage responses of optimized MPPT controller using HPO while coupled with DVPO-FPI controller and DVPO-PI controller in case of pattern 2.

7. Comparison with literature

From previous results, the DVPO-FPI MPPT using HPO is endorsed as an efficient technique for tracking the MPP under a series of experiments. For a massive evaluation of the proposed approach, its response is compared with a set of state-of-the-art MPP techniques from literature, including; incremental conductance(INC) (Zakzouk et al., 2016), Perturb and Observe (P&O) (Nedumgatt et al., 2011), Particle Swarm Optimizer(PSO) (de Oliveira et al., 2016), Grey Wolf Optimizer(GWO) (Mohanty et al., 2015) and Cukoo search algorithm(CSA) (Ahmed and Salam, 2014). Two cases of irradiation levels are accommodated during the comparison stage; the irradiation levels are (550–300–750 W/m^2) and (950–400–650 W/m^2) as illustrated in Fig. 20.

- First case of (550–300–750 W/m^2): Fig. 21 displays the output voltage responses of the different techniques for maximum power point tracking. For the first radiation level in this case(500W/m^2) in Fig. 21(a), it is observed that INC MPPT converges faster than the PSO, GWO, P&O, and CSA techniques in time 0.0826 s with minimal oscillations however, INC does not reach to the voltage level corresponding to the MPP compared to the PSO, GWO, P&O, and CSA. INC converges to a voltage of 352.6V while P&O reaches 352.4V, the stable voltage of GWO is 347V, and CSA and PSO reach the highest stable voltages equal to 355.5V and 353.6 V, respectively. Regarding the proposed optimized DVPO-FPI MPPT-based HPO, it reaches a voltage level of 359.9V at 0.0748 s, affirming its efficiency in achieving the balance between the shortest convergence time and highest stable output voltage for load. As in Fig. 21(a) in the two levels 300W/m^2 and 750W/m^2, the proposed approach also converges to the steady in time less than other approaches and stable voltage higher than other approaches as reported in Table 2.

- Second case of (950–400–650 W/m^2): For more validation for the proposed MPPT approach, another case of radiations of (950–400–650 W/m^2) is applied. The proposed optimized DVPO-FPI MPPT response is compared with MPPT-based GWO, PSO, CSA, INC, and P&O as depicted in Fig. 21(b). The plotted curves illustrate that the proposed approach converges in the shortest time (0.0879 s) and with the highest steady-state output voltage (483.1V) in level (950W/m^2) without any oscillations. Moreover, the optimized DVPO-FPI MPPT displays the same response in the other two of radiation (400W/m^2) and(650W/m^2). Meanwhile, the responses of the PSO, CSA, and GWO show less accuracy in the tracking process with detectable oscillations and long conversion time, as reported in Table 3.

8. Conclusion

From the literature, the previous MPPT techniques have some drawbacks, such as the inability to achieve the balance between getting smooth output without any oscillations and dealing quickly with any sudden changes in environmental conditions. Moreover, needing a huge amount of collective data is another drawback that may impact the time for tracking the MPP. To address these drawbacks, this paper proposes a novel MPPT technique based on the fractional calculus where the fractional PI controller is coupled with the dynamic fractional variable order perturb and observe technique. To adaptively tune the proposed MPPT technique parameters, a nature-inspired optimizer HPO is proposed strategy. To prove the superiority of the proposed technique, it is evaluated through a series of experiments and comparison with integral/fractional PID controllers and a set of state-of-the-art techniques, including MPPT-based

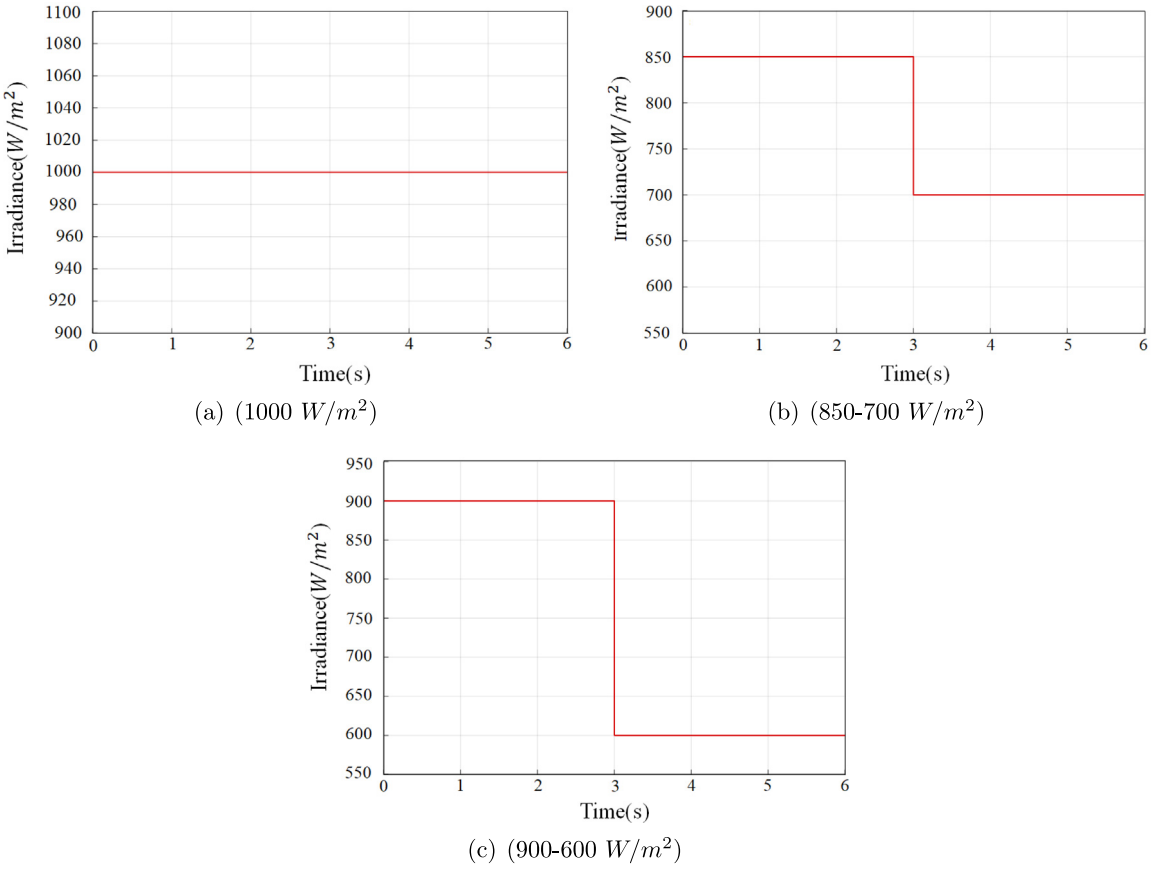

Fig. 18. The radiation levels of (a) pattern 3, (b) pattern 4, and (c) pattern 5.

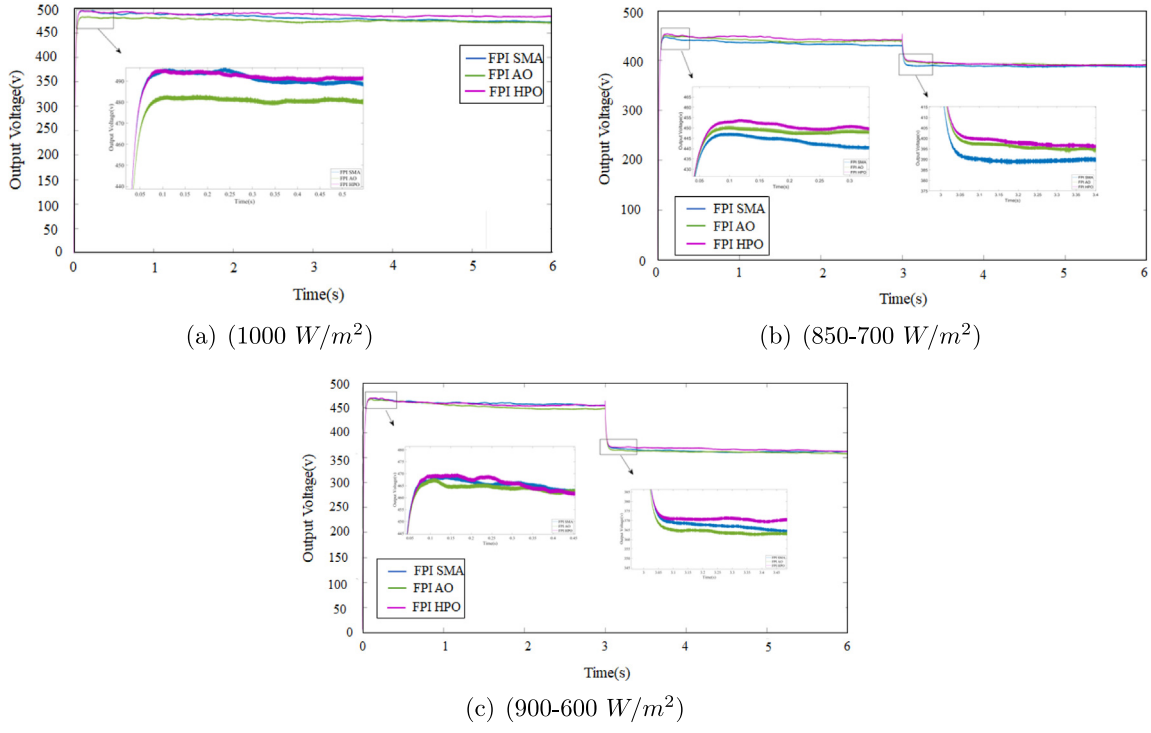

Fig. 19. The output voltages responses of the DVPO-FPI MPPT controllers in cases of (a) SMA, (b) AO, and (c) HPO.

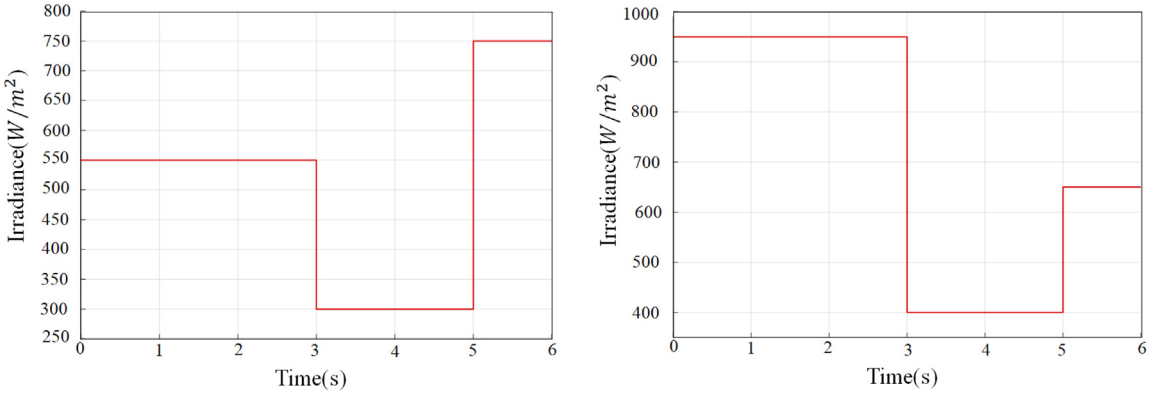

Fig. 20. The radiation levels of (a) pattern 6 and (b) pattern 7.

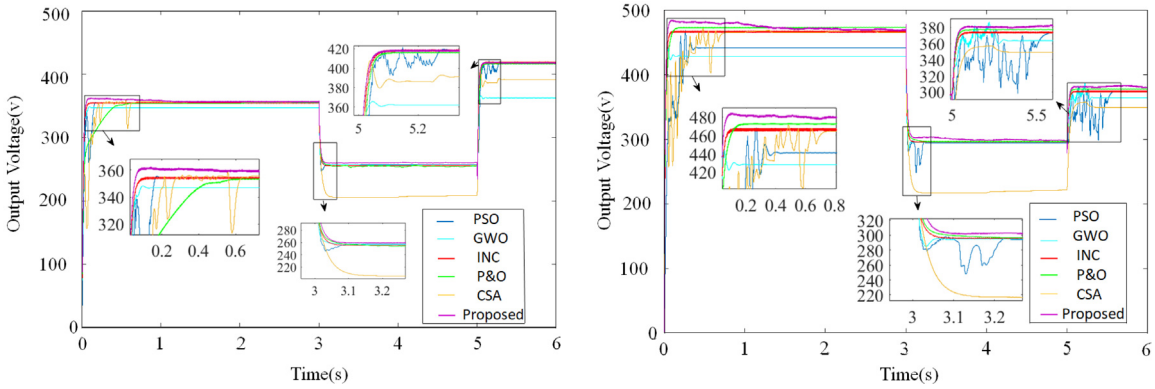

Fig. 21. The output voltages responses of the proposed DVPO-FPI MPPT using HPO and the controllers; P&O (Nedumgatt et al., 2011), PSO (de Oliveira et al., 2016), GWO (Mohanty et al., 2015), INC (Zakzouk et al., 2016), and CSA (Ahmed and Salam, 2014) from the literature.

Table 3
The proposed response versus the literature for the Second case.

Radiation level	Comparison	Proposed	PSO	GWO	INC	P&O	CSA
950 W/m^2	P_{max} (W)	92000	88470	73300	87280	89050	86320
	Time for convergence (s)	0.087	0.436	0.203	0.099	0.1654	0.744
	Oscillation	No	High	Medium	Low	Low	High
400 W/m^2	P_{max} (W)	35850	34270	34670	34980	35130	18780
	Time for convergence (s)	0.077	0.224	0.76	0.08	0.079	0.127
	Oscillation	No	High	Low	No	No	No
650 W/m^2	P_{max} (W)	57920	56460	42160	55530	56980	50850
	Time for convergence (s)	0.063	0.566	0.327	0.068	0.066	0.116
	Oscillation	No	High	Medium	Low	Low	High

slime mold algorithm (SMA), aquila optimizer(AO), incremental conductance (INC), particle swarm optimization(PSO), Grey Wolf Optimizer(GWO), and cuckoo search algorithm (CSA). The comparisons and analyses show the following outcomes

- The proposed DVPO-FPI tuned by HPO proves its ability to respond to the rapid changes in environmental conditions with an efficient and robust detection of MPP with almost zero oscillations during the tracking process.
- The proposed approach convergences in 0.063 s and enhances the tracked power from 4.216×10^4 W, 5.646×10^4 W, 5.085×10^4 W, 5.553×10^4 W and 5.698×10^4 W to 5.792×10^4 W in the cases of using GWO, PSO, CSA, INC, and P&O, respectively that is very close to the theoretical value in level 650 W/m^2 without any oscillations.

For the future work, the dynamic fractional variable order P&O performance can be tested in the MPPT for battery and wind applications.

CRediT authorship contribution statement

Eman Korany: Conceptualization, Methodology, Software, Data curation, Visualization, Formal analysis, Writing – review & editing. **Dalia Yousri:** Conceptualization, Investigation, Writing – review & editing. **Hazem A. Attia:** Conceptualization, Investigation, Writing – review & editing. **Ahmed F. Zobaa:** Conceptualization, Investigation, Writing – review & editing. **Dalia Allam:** Conceptualization, Methodology, Software, Data curation, Visualization, Formal analysis, Editing.

Declaration of competing interest

The authors declare no conflict of interest.

Data availability

No data was used for the research described in the article.

References

A. Elbaset, A., Ali, H., Sattar, A.-E., et al., 2015. A modified perturb and observe algorithm for maximum power point tracking of photovoltaic system using buck-boost converter. JES. J. Eng. Sci. 43 (3), 344–362.

Abdallah, F.S.M., Abdullah, M., Musirin, I., Elshamy, A.M., 2023. Intelligent solar panel monitoring system and shading detection using artificial neural networks. Energy Rep. 9, 324–334.

Aboelela, M.A., Ahmed, M.F., Dorrah, H.T., 2012. Design of aerospace control systems using fractional PID controller. J. Adv. Res. 3 (3), 225–232.

Ahmed, J., Salam, Z., 2014. A maximum power point tracking (MPPT) for PV system using cuckoo search with partial shading capability. Appl. Energy 119, 118–130.

Baimel, D., Tapuchi, S., Levron, Y., Belikov, J., 2019. Improved fractional open circuit voltage MPPT methods for PV systems. Electronics 8 (3), 321.

Baleanu, D., Machado, J.A.T., Luo, A.C., 2011. Fractional Dynamics and Control. Springer Science & Business Media.

Borni, A., Bouarroudj, N., Bouchakour, A., Zaghba, L., 2017. P&O-PI and fuzzy-PI MPPT controllers and their time domain optimization using PSO and GA for grid-connected photovoltaic system: A comparative study. Int. J. Power Electron. 8 (4), 300–322.

Bouakkaz, M.S., Boukadoum, A., Boudebbouz, O., Fergani, N., Boutasseta, N., Attoui, I., Bouraiou, A., Necaibia, A., 2020. Dynamic performance evaluation and improvement of PV energy generation systems using moth flame optimization with combined fractional order PID and sliding mode controller. Sol. Energy 199, 411–424.

Boukezata, B., Chaoui, A., Gaubert, J.-P., Hachemi, M., 2016. An improved fuzzy logic control MPPT based P&O method to solve fast irradiation change problem. J. Renew. Sustain. Energy 8 (4).

Bui, D.M., Le, P.D., Cao, T.M., Nguyen, H.T., Van Tran, T., Nguyen, H.M., 2022. Boost-converter reliability assessment for renewable-energy generation systems in a low-voltage DC microgrid. Energy Rep. 8, 821–835.

de Oliveira, F.M., Oliveira da Silva, S.A., Durand, F.R., Sampaio, L.P., Bacon, V.D., Campanhol, L.B., 2016. Grid-tied photovoltaic system based on PSO MPPT technique with active power line conditioning. IET Power Electron. 9 (6), 1180–1191.

de Dieu Nguimfack-Ndongmo, J., Ngoussandou, B.P., Goron, D., Asoh, D.A., Kidmo, D.K., Nfah, E.M., Kenné, G., 2022. Nonlinear neuro-adaptive MPPT controller and voltage stabilization of PV systems under real environmental conditions. Energy Rep. 8, 1037–1052.

ElSafty, A.H., Tolba, M.F., Said, L.A., Madian, A.H., Radwan, A.G., 2020. A study of the nonlinear dynamics of human behavior and its digital hardware implementation. J. Adv. Res. 25, 111–123.

Fapi, C.B.N., Wira, P., Kamta, M., Tchakounté, H., Colicchio, B., 2021. Simulation and dSPACE hardware implementation of an improved fractional short-circuit current MPPT algorithm for photovoltaic system. Appl. Solar Energy 57, 93–106.

Farayola, A.M., Sun, Y., Ali, A., 2022. Global maximum power point tracking and cell parameter extraction in photovoltaic systems using improved firefly algorithm. Energy Rep. 8, 162–186.

Fathi, M., Parian, J.A., 2021. Intelligent MPPT for photovoltaic panels using a novel fuzzy logic and artificial neural networks based on evolutionary algorithms. Energy Rep. 7, 1338–1348.

Femia, N., Granozio, D., Petrone, G., Spagnuolo, G., Vitelli, M., 2007. Predictive & adaptive MPPT perturb and observe method. IEEE Trans. Aerosp. Electron. Syst. 43 (3), 934–950.

Femia, N., Petrone, G., Spagnuolo, G., Vitelli, M., 2005. Optimization of perturb and observe maximum power point tracking method. IEEE Trans. Power Electron. 20 (4), 963–973.

Hamid, N.F.A., Rahim, N.A., Selvaraj, J., 2016. Solar cell parameters identification using hybrid Nelder-Mead and modified particle swarm optimization. J. Renew. Sustain. Energy 8 (1), 015502.

Hansen, C., 2015. Parameter estimation for single diode models of photovoltaic modules. Tech. Rep.

Hohm, D., Ropp, M.E., 2003. Comparative study of maximum power point tracking algorithms. Prog. Photovolt.: Res. Appl. 11 (1), 47–62.

Hsieh, H.-I., Shih, S.-F., Hsieh, J.-H., Hsieh, G.-C., 2012. A study of high-frequency photovoltaic pulse charger for lead-acid battery guided by PI-INC MPPT. In: 2012 International Conference on Renewable Energy Research and Applications. ICRERA, IEEE, pp. 1–6.

Hussein, K., Muta, I., Hoshino, T., Osakada, M., 1995. Maximum photovoltaic power tracking: An algorithm for rapidly changing atmospheric conditions. IEE Proc., Gener. Transm. Distrib. 142 (1), 59–64.

Jiang, Y., Qahouq, J.A.A., Haskew, T.A., 2012. Adaptive step size with adaptive-perturbation-frequency digital mppt controller for a single-sensor photovoltaic solar system. IEEE Trans. Power Electron. 28 (7), 3195–3205.

Jyothy, L.P., Sindhu, M., 2018. An artificial neural network based MPPT algorithm for solar PV system. In: 2018 4th International Conference on Electrical Energy Systems. ICEES, IEEE, pp. 375–380.

Kang, T., Yao, J., Jin, M., Yang, S., Duong, T., 2018. A novel improved cuckoo search algorithm for parameter estimation of photovoltaic (PV) models. Energies 11 (5), 1060.

Manna, S., Singh, D.K., Akella, A.K., Kotb, H., AboRas, K.M., Zawbaa, H.M., Kamel, S., 2023. Design and implementation of a new adaptive MPPT controller for solar PV systems. Energy Rep. 9, 1818–1829.

Mao, M., Cui, L., Zhang, Q., Guo, K., Zhou, L., Huang, H., 2020. Classification and summarization of solar photovoltaic MPPT techniques: A review based on traditional and intelligent control strategies. Energy Rep. 6, 1312–1327.

Mo, S., Ye, Q., Jiang, K., Mo, X., Shen, G., 2022. An improved MPPT method for photovoltaic systems based on mayfly optimization algorithm. Energy Rep. 8, 141–150.

Mohanty, S., Subudhi, B., Ray, P.K., 2015. A new MPPT design using grey wolf optimization technique for photovoltaic system under partial shading conditions. IEEE Trans. Sustain. Energy 7 (1), 181–188.

Narendiran, S., Sahoo, S.K., Das, R., Sahoo, A.K., 2016. Fuzzy logic controller based maximum power point tracking for pv system. In: 2016 3rd International Conference on Electrical Energy Systems. ICEES, IEEE, pp. 29–34.

Naruei, I., Keynia, F., Sabbagh Molahosseini, A., 2022. Hunter–prey optimization: Algorithm and applications. Soft Comput. 26 (3), 1279–1314.

Nedumgatt, J.J., Jayakrishnan, K., Umashankar, S., Vijayakumar, D., Kothari, D., 2011. Perturb and observe MPPT algorithm for solar PV systems-modeling and simulation. In: 2011 Annual IEEE India Conference. IEEE, pp. 1–6.

Pandey, A., Dasgupta, N., Mukerjee, A.K., 2007. A simple single-sensor MPPT solution. IEEE Trans. Power Electron. 22 (2), 698–700.

Pandey, A., Dasgupta, N., Mukerjee, A.K., 2008. High-performance algorithms for drift avoidance and fast tracking in solar MPPT system. IEEE Trans. Energy Convers. 23 (2), 681–689.

Phang, J., Chan, D., Phillips, J., 1984. Accurate analytical method for the extraction of solar cell model parameters. Electron. Lett. 10 (20), 406–408.

Piegari, L., Rizzo, R., 2010. Adaptive perturb and observe algorithm for photovoltaic maximum power point tracking. IET Renew. Power Gener. 4 (4), 317–328.

Pilakkat, D., Kanthalakshmi, S., 2020. Single phase PV system operating under partially shaded conditions with ABC-PO as MPPT algorithm for grid connected applications. Energy Rep. 6, 1910–1921.

Prasad, T.N., Devakirubakaran, S., Muthubalaji, S., Srinivasan, S., Karthikeyan, B., Palanisamy, R., Bajaj, M., Zawbaa, H.M., Kamel, S., 2022. Power management in hybrid ANFIS PID based AC–DC microgrids with EHO based cost optimized droop control strategy. Energy Rep. 8, 15081–15094.

Ramadan, H.A., Khan, B., Diab, A.A.Z., 2022. Accurate parameters estimation of three diode model of photovoltaic modules using hunter–prey and wild horse optimizers. IEEE Access 10, 87435–87453.

Reisi, A.R., Moradi, M.H., Jamasb, S., 2013. Classification and comparison of maximum power point tracking techniques for photovoltaic system: A review. Renew. Sustain. Energy Rev. 19, 433–443.

Rezk, H., Eltamaly, A.M., 2015. A comprehensive comparison of different MPPT techniques for photovoltaic systems. Solar Energy 112, 1–11.

Sahoo, J., Samanta, S., Bhattacharyya, S., 2020. Adaptive PID controller with P&O MPPT algorithm for photovoltaic system. IETE J. Res. 66 (4), 442–453.

Sahu, R.K., Shaw, B., 2018. Design of solar system by implementing ALO optimized PID based mppt controller. Trends Renew. Energy 4 (3), 44–55.

Salameh, Z.M., Dagher, F., Lynch, W.A., 1991. Step-down maximum power point tracker for photovoltaic systems. Sol. Energy 46 (5), 279–282.

Schoeman, J., Van Wyk, J., 1982. A simplified maximal power controller for terrestrial photovoltaic panel arrays. In: 1982 IEEE Power Electronics Specialists Conference. IEEE, pp. 361–367.

Sera, D., Teodorescu, R., Hantschel, J., Knoll, M., 2008. Optimized maximum power point tracker for fast changing environmental conditions. In: 2008 IEEE International Symposium on Industrial Electronics. pp. 2401–2407. http://dx.doi.org/10.1109/ISIE.2008.4677275.

Soliman, N.S., Tolba, M.F., Said, L.A., Madian, A.H., Radwan, A.G., 2019. Fractional X-shape controllable multi-scroll attractor with parameter effect and FPGA automatic design tool software. Chaos Solitons Fractals 126, 292–307.

Toumi, D., Benattous, D., Ibrahim, A., Abdul-Ghaffar, H., Obukhov, S., Aboelsaud, R., Labbi, Y., Diab, A.A.Z., 2021. Optimal design and analysis of DC–DC converter with maximum power controller for stand-alone PV system. Energy Rep. 7, 4951–4960.

Wang, X., Li, J., Shao, L., Liu, H., Ren, L., Zhu, L., 2023. Short-term wind power prediction by an extreme learning machine based on an improved hunter–prey optimization algorithm. Sustainability 15 (2), 991.

Wasim, M.S., Amjad, M., Habib, S., Abbasi, M.A., Bhatti, A.R., Muyeen, S., 2022. A critical review and performance comparisons of swarm-based optimization algorithms in maximum power point tracking of photovoltaic systems under partial shading conditions. Energy Rep. 8, 4871–4898.

Wasynezuk, O., 1983. Dynamic behavior of a class of photovoltaic power systems. IEEE Trans. Power Appar. Syst. PAS-102 (9), 3031–3037. http://dx.doi.org/10.1109/TPAS.1983.318109.

Won, C.-Y., Kim, D.-H., Kim, S.-C., Kim, W.-S., Kim, H.-S., 1994. A new maximum power point tracker of photovoltaic arrays using fuzzy controller. In: Proceedings of 1994 Power Electronics Specialist Conference-PESC'94, Vol. 1. IEEE, pp. 396–403.

Yang, B., Yu, T., Zhang, X., Li, H., Shu, H., Sang, Y., Jiang, L., 2019a. Dynamic leader based collective intelligence for maximum power point tracking of PV systems affected by partial shading condition. Energy Convers. Manage. 179, 286–303.

Yang, B., Zhong, L., Zhang, X., Shu, H., Yu, T., Li, H., Jiang, L., Sun, L., 2019b. Novel bio-inspired memetic salp swarm algorithm and application to MPPT for PV systems considering partial shading condition. J. Clean. Prod. 215, 1203–1222.

Yang, B., Zhu, T., Wang, J., Shu, H., Yu, T., Zhang, X., Yao, W., Sun, L., 2020. Comprehensive overview of maximum power point tracking algorithms of PV systems under partial shading condition. J. Clean. Prod. 268, 121983.

Zaghba, L., Khennane, M., Borni, A., Fezzani, A., Bouchakour, A., Mahammed, I.H., Oudjana, S.H., 2019. A genetic algorithm based improve P&O-PI MPPT controller for stationary and tracking grid-connected photovoltaic system. In: 2019 7th International Renewable and Sustainable Energy Conference. IRSEC, IEEE, pp. 1–6.

Zakzouk, N.E., Elsaharty, M.A., Abdelsalam, A.K., Helal, A.A., Williams, B.W., 2016. Improved performance low-cost incremental conductance PV MPPT technique. IET Renew. Power Gener. 10 (4), 561–574.